

Initial state dependence of the quench dynamics in integrable quantum systems

Marcos Rigol¹ and Mattias Fitzpatrick^{1,2}

¹*Department of Physics, Georgetown University, Washington, DC 20057, USA*

²*Department of Physics, Middlebury College, Middlebury, Vermont 05753, USA*

We identify and study classes of initial states in integrable quantum systems that, after the relaxation dynamics following a sudden quench, lead to near-thermal expectation values of few-body observables. In the systems considered here, those states are found to be insulating ground states of lattice hard-core boson Hamiltonians. We show that, as a suitable parameter in the initial Hamiltonian is changed, those states become closer to Fock states (products of single site states) as the outcome of the relaxation dynamics becomes closer to the thermal prediction. At the same time, the energy density approaches a Gaussian. Furthermore, the entropy associated with the generalized canonical and generalized grand-canonical ensembles, introduced to describe observables in integrable systems after relaxation, approaches that of the conventional canonical and grand-canonical ensembles. We argue that those classes of initial states are special because a control parameter allows one to tune the distribution of conserved quantities to approach the one in thermal equilibrium. This helps in understanding the approach of all the quantities studied to their thermal expectation values. However, a finite-size scaling analysis shows that this behavior should not be confused with thermalization as understood for nonintegrable systems.

PACS numbers: 02.30.Ik, 05.30.-d, 03.75.Kk, 05.30.Jp

I. INTRODUCTION

The relaxation dynamics of isolated quantum systems after a sudden quench is a topic that is attracting much current attention. Interest on this problem has been sparked by recent experiments with ultracold gases [1–4]. The high degree of isolation in those experiments allows one to consider them as almost ideal analog simulators of the unitary dynamics of pure quantum states. For example, in Ref. [2], Kinoshita *et al.* showed that observables in a (quasi)-one-dimensional bosonic system close to an integrable point do not relax to the values expected from a conventional statistical mechanics description. Any non-negligible coupling to a thermal environment would have destroyed such a remarkable phenomenon. More recently, Trotzky *et al.* [4] have shown that the experimental dynamics of Bose-Hubbard like (quasi)-one-dimensional systems can be almost perfectly described by the unitary dynamics of the relevant model Hamiltonian. The latter was followed by numerically exact means utilizing the time-dependent renormalization group algorithm [5, 6].

After the experimental results in Ref. [2], many theoretical works have found that, following a sudden quench within integrable systems, few-body observables, in general, relax to nonthermal expectation values [7–23] (for a recent review, see Ref. [24]). Some of the novel insights gained through these studies include (i) the possibility of describing observables after relaxation by means of generalized Gibb ensembles (GGE) [7–14, 16–18, 21–23]; (ii) the fact that even though in some cases the behavior of nonlocal observables after relaxation can be parametrized similarly to the one in thermal equilibrium [15, 20], an exact description of those observables is provided only by the GGE [22], and (iii) an understanding of the GGE through a generalization of the eigenstate thermalization

hypothesis (ETH) [21]. ETH explains why thermalization occurs in generic (nonintegrable) quantum systems after a quench [25–27].

All the results discussed above have been obtained in studies of several specific models. However, they are expected to hold in general for integrable systems. An interesting, and so far nongeneric, result reported in Refs. [8, 21] was the observation of a phenomenon close to “real” thermalization in integrable systems, in the sense of the expectation values of few-body observables after relaxation approaching those predicted in thermal equilibrium. This occurred as a parameter used to generate special classes of initial states was changed. In Ref. [8], the initial states were insulating ground states of hard-core bosons in half-filled period-two superlattices, while in Ref. [21], they were the ground state of trapped systems with a Mott insulating domain in the trap center.

In this work, we revisit the systems above and focus on understanding the properties of the initial states for which observables after relaxation were seen to approach thermal expectation values, despite integrability. As said before, those states are insulating ground states. Here, we show that the selected tuning parameter makes those initial states approach Fock states (products of single site wavefunctions) at the same time that (i) their energy density approaches a Gaussian, and (ii) the entropy of their associated generalized canonical and grand-canonical ensembles approach the entropies of the canonical and grand-canonical ensembles. We argue that (i) and (ii) above can be understood because the distribution of conserved quantities in such initial states approaches the one of systems in thermal equilibrium. Hence, they can have thermal-like energy densities, entropies, and observables after relaxation. However, after a finite-size scaling analysis, we conclude that this phenomenon differs conceptually from thermalization as it happens in non-

tegrable systems.

The presentation is organized as follows: in Sec. II, we introduce the models and observables of interest. We also define the ensembles considered and provide details on how the calculations are performed. Section III is devoted to study of the overlaps of the initial states with the eigenstates of the final Hamiltonians, as well as to the description of the energy densities in all cases. The scaling of the entropy with system size, for the different ensembles analyzed and for superlattice and trapped systems, is presented in Sec. IV. In Sec. V, we study the distribution of the conserved quantities for the different initial states and within standard statistical ensembles. Finally, the conclusions are presented in Sec. VI.

II. MODEL, ENSEMBLES, AND OBSERVABLES

We are interested in the equilibrium and nonequilibrium properties of lattice bosons in the limit of infinite on-site repulsion (hard-core bosons). Those systems can be described by the Hamiltonian

$$\hat{H} = -J \sum_{j=1}^{L-1} \left(\hat{b}_j^\dagger \hat{b}_{j+1} + \text{H.c.} \right) + \sum_{j=1}^L V_j^{\text{ext}} \hat{n}_j, \quad (1)$$

with the additional on-site constraints $\hat{b}_j^{\dagger 2} = \hat{b}_j^2 = 0$, which preclude multiple occupancy of the lattice sites. Here, J is the nearest-neighbor hopping, V_j^{ext} is a site-dependent local potential, and L is the number of lattice sites. The hard-core boson creation (annihilation) operator in each site is denoted by \hat{b}_j^\dagger (\hat{b}_j) and the site number occupation by $\hat{n}_j = \hat{b}_j^\dagger \hat{b}_j$. In what follows, we consider only systems with open boundary conditions, and $t = 1$ sets our units of energy.

This model is integrable [28] and can be exactly solved by first mapping it onto the spin-1/2 XX model (with a site-dependent magnetic field in the z direction) by means of the Holstein-Primakoff transformation [29] and then onto a noninteracting fermion Hamiltonian utilizing the Jordan-Wigner transformation [28, 30]. In the fermionic language, the Hamiltonian can be straightforwardly diagonalized and all the spectral and thermodynamic properties of hard-core bosons can be computed either analytically or numerically in polynomial time. Off-diagonal correlations are more difficult to calculate. However, using properties of Slater determinants, they can also be computed very efficiently numerically for ground state [31, 32] and finite temperature [33] equilibrium problems, as well as during the unitary nonequilibrium dynamics [34]. Those insights will be used later.

More generally, the nonequilibrium dynamics of isolated quantum systems can be studied by writing the (arbitrary) initial state $|\psi_I\rangle$ as a linear combination of the eigenstates $|\Psi_\alpha\rangle$ of the Hamiltonian \hat{H} that drives

the dynamics, which satisfies $\hat{H}|\Psi_\alpha\rangle = E_\alpha|\Psi_\alpha\rangle$. Hence,

$$|\psi_I\rangle = \sum_{\alpha=1}^D C_\alpha |\Psi_\alpha\rangle, \quad (2)$$

where D is the dimension of the Hilbert space and $C_\alpha = \langle \Psi_\alpha | \psi_I \rangle$, and the time evolving wave function can be written as

$$|\Psi(t)\rangle = e^{-i\hat{H}t/\hbar} |\psi_I\rangle = \sum_{\alpha=1}^D C_\alpha e^{-iE_\alpha t/\hbar} |\Psi_\alpha\rangle. \quad (3)$$

The time evolution of a generic observable \hat{O} is then dictated by the sums over all eigenstates

$$\langle \hat{O}(t) \rangle = \langle \Psi(t) | \hat{O} | \Psi(t) \rangle = \sum_{\alpha,\beta} C_\alpha^* C_\beta e^{i(E_\alpha - E_\beta)t/\hbar} O_{\alpha\beta}, \quad (4)$$

where $O_{\alpha\beta} = \langle \Psi_\alpha | \hat{O} | \Psi_\beta \rangle$, and the infinite time average of Eq. (4) (in the absence of degeneracies) can be thought as the result of a diagonal ensemble average [27]

$$\langle \hat{O} \rangle_{\text{DE}} = \sum_{\alpha} |C_\alpha|^2 O_{\alpha\alpha}. \quad (5)$$

As shown in Refs. [21, 27], this infinite time average describes observables after relaxation. We should stress that this can be true even in the presence of degeneracies associated with integrability, except for cases with massive degeneracies [14]. The validity of the description of integrable systems after relaxation, by means of the infinite time average (5), has been demonstrated for the $1/r$ Hubbard model in Ref. [14], and for the same (hard-core boson) systems considered here in Ref. [21] (supplementary materials).

The result in Eq. (5) is to be compared with the predictions of conventional statistical mechanics ensembles, for a system in equilibrium with energy $E_I = \langle \psi_I | \hat{H} | \psi_I \rangle$ and total number of particles N . The canonical ensemble predicts

$$\langle \hat{O} \rangle_{\text{CE}} = \frac{1}{Z_{\text{CE}}} \sum_{\alpha} e^{-E_\alpha/k_B T} O_{\alpha\alpha}, \quad (6)$$

where $Z_{\text{CE}} = \sum_{\alpha} e^{-E_\alpha/k_B T}$, T needs to be taken such that $E_I = Z_{\text{CE}}^{-1} \sum_{\alpha} e^{-E_\alpha/k_B T} E_\alpha$, and the sums run over all eigenstates of the Hamiltonian (with energy E_α) in the sector with N particles. The grand-canonical ensemble, on the other hand, predicts

$$\langle \hat{O} \rangle_{\text{GE}} = \frac{1}{Z_{\text{GE}}} \sum_{\alpha} e^{-(E_\alpha - \mu N_\alpha)/k_B T} O_{\alpha\alpha}, \quad (7)$$

where $Z_{\text{GE}} = \sum_{\alpha} e^{-(E_\alpha - \mu N_\alpha)/k_B T}$, T and μ need to be taken such that $E_I = Z_{\text{GE}}^{-1} \sum_{\alpha} e^{-(E_\alpha - \mu N_\alpha)/k_B T} E_\alpha$ and $N = Z_{\text{GE}}^{-1} \sum_{\alpha} e^{-(E_\alpha - \mu N_\alpha)/k_B T} N_\alpha$, and the sums run over all eigenstates of the Hamiltonian (with energy E_α and

number of particles N_α). The predictions of Eq. (6) and Eq. (7) in general agree in the thermodynamic limit.

Thermalization is then said to occur if, for sufficiently large systems, $\langle \hat{O} \rangle_{\text{DE}} \simeq \langle \hat{O} \rangle_{\text{CE}} \simeq \langle \hat{O} \rangle_{\text{GE}}$. Hence, the fact that thermalization occurs in isolated systems is surprising as $\langle \hat{O} \rangle_{\text{DE}}$ depends on the initial conditions through the projection of the initial state onto all the eigenstates of the Hamiltonian, while conventional statistical ensembles depend only on the initial conditions through E_I and N . Since the energy distribution of the initial state $|\psi_I\rangle$ in the eigenstates of the final Hamiltonian is narrow (because of locality, see Ref. [27] and its supplementary materials) and centered around E_I , similarly to the canonical and grand-canonical ensembles, then thermalization can be understood to occur because of ETH [25–27]. ETH states that in generic many-body systems $O_{\alpha\alpha}$ almost do not fluctuate between eigenstates that have similar energies, i.e., the eigenstates themselves already exhibit thermal behavior.

Furthermore, it has been also proposed that one can define the entropy of the isolated system after the quench to be the diagonal entropy [35]

$$S_d = - \sum_{\alpha} |C_{\alpha}|^2 \ln(|C_{\alpha}|^2), \quad (8)$$

which satisfies all the thermodynamic properties required from an entropy. Indeed, this entropy has been recently shown to be consistent with the microcanonical entropy for nonintegrable systems [36], and hence, for sufficiently large systems it is expected to agree with the entropy of the canonical ensemble

$$S_{\text{CE}} = \ln Z_{\text{CE}} + \frac{E_I}{k_B T}, \quad (9)$$

and with that of the grand-canonical ensemble

$$S_{\text{GE}} = \ln Z_{\text{GE}} + \frac{E_I - \mu N}{k_B T}, \quad (10)$$

up to subextensive corrections.

In general, in integrable systems such as the ones of interest in this work, the presence of a complete set of conserved quantities prevents thermalization [7, 27]. (The eigenstate thermalization hypothesis has been shown to fail in those systems [21, 27].) However, after relaxation, few-body observables can be described by means of a generalization of the Gibbs ensemble [7], with a density matrix

$$\hat{\rho}_{\text{GGE}} = Z_{\text{GGE}}^{-1} e^{-\sum_n \lambda_n \hat{I}_n}, \quad (11)$$

where $Z_{\text{GGE}} = \text{Tr} \left[e^{-\sum_n \lambda_n \hat{I}_n} \right]$, $\{\hat{I}_n\}$ are the conserved quantities, and $n = 1, \dots, L$. In our systems, $\{\hat{I}_n\}$ are the occupation operators of the single-particle eigenstates of the noninteracting fermionic Hamiltonian to which hard-core bosons can be mapped. $\{\lambda_n\}$ are the Lagrange multipliers, which are selected such that $\langle \psi_I | \hat{I}_n | \psi_I \rangle =$

$\text{Tr}(\hat{I}_n \hat{\rho}_{\text{GGE}})$. For hard-core bosons, they can be computed using the expression [7]

$$\lambda_n = \ln \left[\frac{1 - \langle \psi_I | \hat{I}_n | \psi_I \rangle}{\langle \psi_I | \hat{I}_n | \psi_I \rangle} \right] \quad (12)$$

and Z_{GGE} is then

$$Z_{\text{GGE}} = \prod_n (1 + e^{-\lambda_n}). \quad (13)$$

The fact that the GGE is able to predict expectation values of few-body observables after relaxation can be understood in terms of a generalized ETH [21]. The idea in this case is that eigenstates of the Hamiltonian that have similar values of the conserved quantities have similar expectation values of few-body observables. The GGE is then the ensemble that, within the full spectrum, selects a narrow set of states with the same distribution of conserved quantities that is fixed by the initial state.

The GGE entropy is given by

$$S_{\text{GGE}} = \ln Z_{\text{GGE}} + \sum_n \lambda_n \langle \psi_I | \hat{I}_n | \psi_I \rangle. \quad (14)$$

Furthermore, one can also define a canonical version of this generalized ensemble, with a density matrix

$$\hat{\rho}_{\text{GCE}} = Z_{\text{GCE}}^{-1} e^{-\sum_n \lambda_n \hat{I}_n}, \quad (15)$$

for which only states with N particles are considered when calculating traces. We keep λ_n in the sector with N particles to have the same values as within the GGE and take the partition function to be the trace over states with N particles, $Z_{\text{GCE}} = \text{Tr} \left[e^{-\sum_n \lambda_n \hat{I}_n} \right]_N$. The entropy of this ensemble can be computed as

$$S_{\text{GCE}} = \text{Tr}[\hat{\rho}_{\text{GCE}} \ln(\hat{\rho}_{\text{GCE}})]_N \quad (16)$$

where, once again, only eigenstates of the Hamiltonian with N particles contribute to the trace.

An interesting recent finding in Ref. [36] was that despite the fact that the generalized ensembles do describe few-body observables in integrable systems after relaxation, their entropy is always greater than that of the diagonal ensemble, and the difference increases linearly with increasing system size. This means that an exponentially larger number of states contribute to the generalized ensembles when compared to the diagonal one. The generalized ETH ensures that, despite having a much greater number of states, the generalized ensembles predict the outcome of the realization dynamics. This is because the overwhelming majority of the states that contribute to the generalized ensembles have identical expectation values of few-body observables as the ones that contribute to the diagonal ensemble [21]. All these results are expected to be generic in integrable systems.

In this work, instead, we focus on special classes of initial states that lead to expectation values of few-body

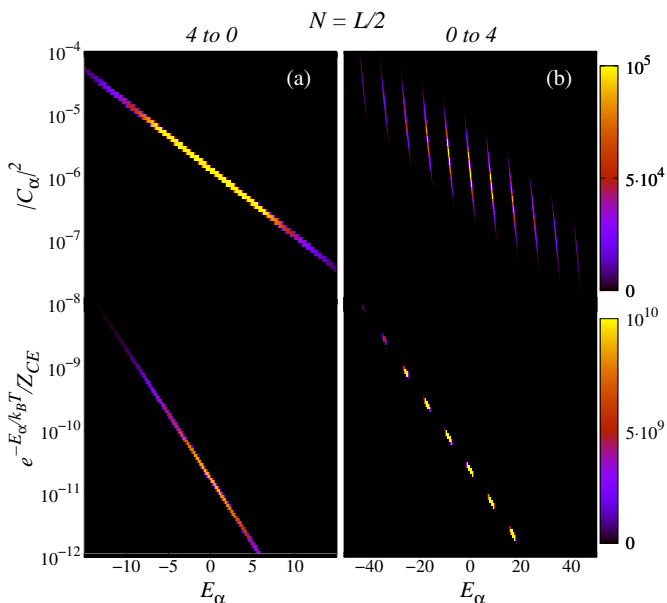


FIG. 1: (Color online) Weights of the eigenstates of the final Hamiltonian in the diagonal (top half in both panels) and canonical (bottom half in both panels) ensembles, $|C_\alpha|^2$ and $e^{-E_\alpha/k_B T}/Z_{CE}$, respectively, for $L = 36$ and $N = 18$ (half filling). The panel on the left (a) depicts results for a quench from $A_I = 4$ to $A_F = 0$, and the panel on the right (b) for a quench from $A_I = 0$ to $A_F = 4$. In both cases, we select the initial state to be the ground state of Eq. (1) for the given value of $A = A_I$. The color scale indicates the number of states, per unit area in the plot, that have a given weight.

observables that approach those in thermal equilibrium, despite integrability [8, 21]. Since we know that ETH is not satisfied in those systems [21, 27], the fact that observables after relaxation approach thermal values then must be related to special properties of the overlaps C_α of the initial states with the eigenstates of the final Hamiltonians. Hence, we study the behavior of the C_α 's in such systems. Hard-core bosons can be mapped onto noninteracting fermions, so one can generate the exponentially large Hilbert space of finite systems [whose size is $\binom{L}{N}$] without the need of diagonalizing the full Hamiltonians. Those many-body states are created as products of noninteracting fermionic eigenstates. They can be written as Slater determinants, in terms of fermionic creation operators \hat{f}_k^\dagger , as

$$|\Psi_\alpha\rangle = \prod_{l=1}^N \sum_{k=1}^L P_{kl}^\alpha \hat{f}_k^\dagger |0\rangle, \quad (17)$$

and the same can be done for the initial state $|\Psi_I\rangle = \prod_{l=1}^N \sum_{k=1}^L P_{kl}^0 \hat{f}_k^\dagger |0\rangle$. The overlap between the initial state and the eigenstates of the final Hamiltonian can then be calculated numerically as the determinant of the product of two matrices [31, 32]

$$C_\alpha = \langle \Psi_\alpha | \Psi_I \rangle = \det \left[(\mathbf{P}^\alpha)^\dagger \mathbf{P}^0 \right], \quad (18)$$

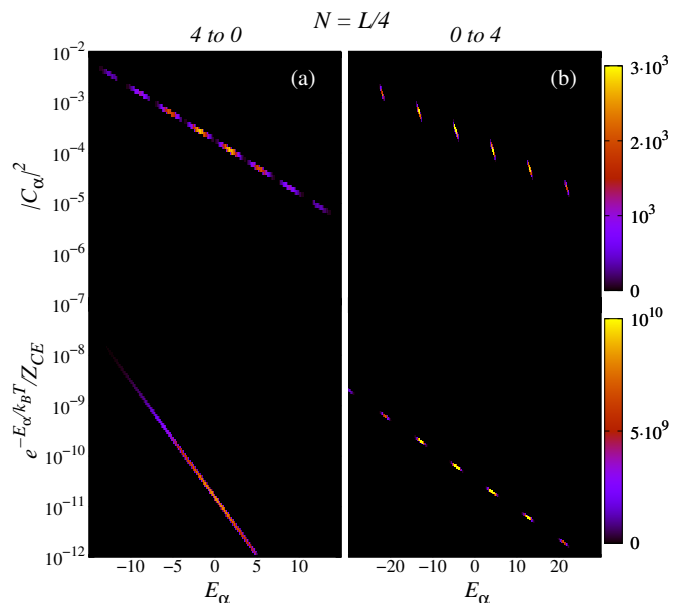


FIG. 2: (Color online) Same as Fig. 1 but for $L = 44$ and $N = 11$ (quarter filling).

which, together with all the expressions presented previously, allow us to compute the energy distributions and entropies in the diagonal, canonical, grand-canonical, and generalized ensembles.

III. OVERLAPS

We first focus on the behavior of the weights $|C_\alpha|^2$ determined by the initial state and compare it with the one given by the canonical ensemble $e^{-E_\alpha/k_B T}/Z_{CE}$. Most of the results reported in this manuscript are obtained from calculations for superlattices with period two. What that means is that in Eq. (1),

$$V_j^{\text{ext}} = A(-1)^j.$$

We will mainly focus on fillings (i) $N = L/2$ (half filling), for which observables after relaxation were seen to quickly approach the thermal predictions when the value of A_I was increased and $A_F = 0$, but no such thing was observed when $A_I = 0$ and A_F was increased [8], and (ii) $N = L/4$ (quarter filling), which does not exhibit an approach to the thermal predictions, like the one seen at half filling, no matter the selected values of A_I and A_F . Some results for trapped systems, related to the findings in Ref. [21], will be reported in the following section.

By comparing Eqs. (5) and (6), one may naively think that for those states for which an approach to thermal expectation values was observed, the weights of the initial state in the eigenstates of the final Hamiltonian $|C_\alpha|^2$ may approach those of the canonical ensemble $e^{-E_\alpha/k_B T}/Z_{CE}$. In Fig. 1, we plot the values of $|C_\alpha|^2$ (top half in both panels) and $e^{-E_\alpha/k_B T}/Z_{CE}$ (bottom half in both panels) for quenches from the ground state

of a superlattice ($A_I = 4$) to the homogeneous lattice ($A_F = 0$) (a) and from the ground state of the homogeneous lattice ($A_I = 0$) to the superlattice ($A_F = 4$) (b).

Figure 1 clearly shows that the actual values of $|C_\alpha|^2$ differ not only quantitatively (several orders of magnitude) from those of $e^{-E_\alpha/k_B T}/Z_{\text{CE}}$ but also qualitatively different for both quenches, as the former exhibit a slower decay with the energy of the eigenstates. No convergence between the values of $|C_\alpha|^2$ and $e^{-E_\alpha/k_B T}/Z_{\text{CE}}$ is observed as A_I and A_F are changed (not shown). In Fig. 1, we also provide information about the number of states, per unit area in the plot, that have a given weight within in each ensemble (color scale). For the quench from $A_I = 4$ to $A_F = 0$, one can see in Fig. 1(a) (top half) that the number of states with nonzero values of $|C_\alpha|^2$ continuously increases as the energy increases and reaches a maximum around the center of the spectrum, where the density of states is largest. A similar behavior can be seen within the canonical ensemble in Fig. 1(a) (bottom half). For the quenches from $A_I = 0$ to $A_F = 4$, on the other hand, there are isolated islands with nonzero weights both in the diagonal and canonical ensembles [Fig. 1(b)]. This is because the many-body spectrum exhibits bands of eigenstates separated by gaps, which are determined by the value of A_F . Such a behavior can be straightforwardly understood from the single-particle band structure. In the periodic case, a reasonably good approximation for large systems with open boundary conditions, the latter exhibits two bands given by the expression

$$\epsilon_\pm(k) = \pm \sqrt{4t^2 \cos^2(ka) + A^2}, \quad (19)$$

where “+” denotes the upper band and “-” the lower band and k is the single particle momentum. Depending on which values of k are occupied in the many-body state, the bands seen in Fig. 1(b) form.

Results for the same quenches as in Fig. 1, but for quarter-filled systems, are presented in Fig. 2. The latter are qualitatively similar to the former in everything, except for the behavior of the number of eigenstates with nonzero values of $|C_\alpha|^2$ in the quenches from $A_I = 4$ to $A_F = 0$ [top half in Fig. 2(a)]. At quarter filling, when $A_I = 4$, the initial state imprints a modulation on the number of eigenstates with nonzero $|C_\alpha|^2$ (note that the spectrum in the final Hamiltonian, when $A_F = 0$, has no gaps). That modulation is not present for the quenches at half filling [top half in Fig. 1(a)] and, as expected (because of the continuous spectrum of the final Hamiltonian), it is not present in the canonical results in the bottom half of Fig. 2(a).

The fact that the weights in the diagonal and canonical (or any other) ensemble differ from each other is generic for integrable and nonintegrable systems [37] and, as such, need not preclude thermalization. After all, the weights with which eigenstates of the Hamiltonian contribute to the canonical and microcanonical ensembles also differ. The relevant quantity to compare different

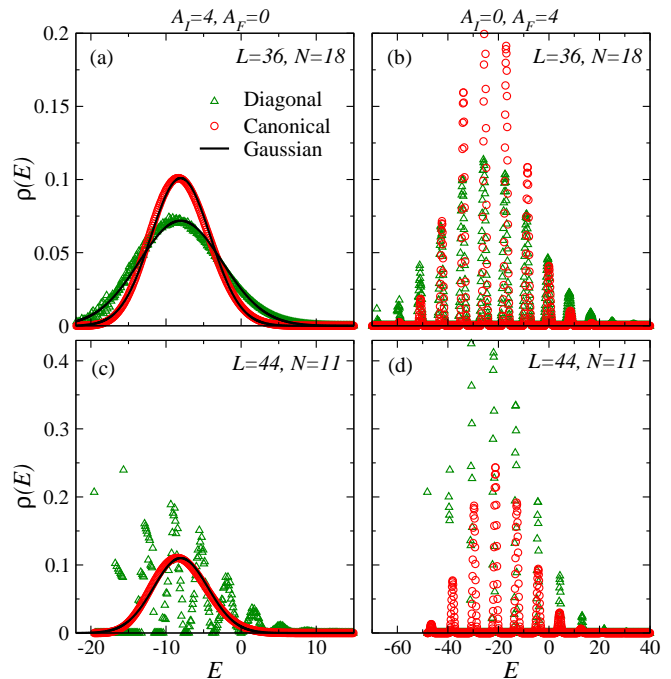


FIG. 3: (Color online) Energy density $\rho(E)$ for the quenches depicted in Figs. 1 and 2. Results are presented for the case $A_I = 4$, $A_F = 0$ in the left panels [(a) and (c)] and for $A_I = 0$, $A_F = 4$ in the right panels [(b) and (d)] and for systems at half filling [(a) and (b)] and at quarter filling [(c) and (d)]. $\rho(E)$ is reported for the diagonal and canonical ensembles, and, when appropriate, we have fitted the results to a Gaussian (continuous lines in the plots). In all cases $\delta E = 0.1$.

ensembles is the energy density $\rho(E)$, which is equal to the sum of the weights studied in Figs. 1 and 2, over a given energy window δE , divided by δE . By construction, the integral of this quantity over the full energy spectrum is normalized to 1. (δE needs to be selected in such a way that the results for the energy density are independent of its actual value.) The energy density depends not only on the weights but also on the density of states, and tells us which part of the spectrum is the one that contributes the most to the ensemble averages.

In Fig. 3, we present $\rho(E)$ for the quenches for which the weights of the diagonal and canonical ensembles were reported in Figs. 1 and 2. As expected, the energy density in the canonical ensemble is very close to a Gaussian $\rho(E) = (\sqrt{2\pi}\delta E)^{-1} e^{-(E-E_I)^2/(2\delta E^2)}$ in all cases. For the quenches from $A_I = 0$ to $A_F = 4$, the Gaussian is cut by the bands described previously.

In diagonal ensemble, $\rho(E)$ has been recently shown to be very well described by a Gaussian for nonintegrable systems and sparse (very different from Gaussian) in integrable systems [36]. We find the latter to be generic for our quenches, as shown in Figs. 3(c), 3(d), and, maybe less evident but still true, Fig. 3(b). Surprisingly, we find that for quenches from $A_I \neq 0$ to $A_F = 0$ at half filling, the energy density in the diagonal ensemble approaches a Gaussian as the value of A_I is increased. See Fig. 3(a)

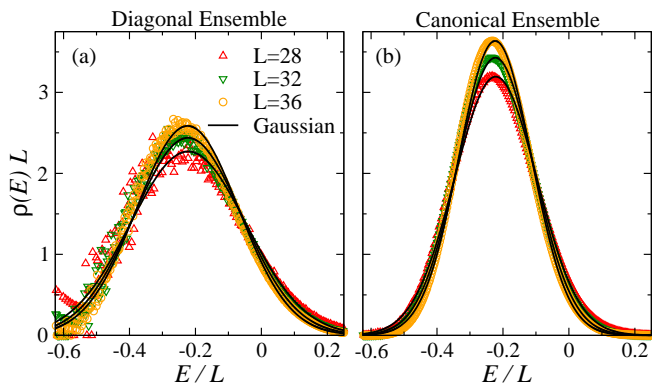


FIG. 4: (Color online) Scaling of the energy density in the diagonal (a) and canonical ensembles (b) with increasing system size. Results are reported for the quenches from $A_I = 4$ to $A_F = 0$ at half filling. Continuous lines depict the result of the fit of each data set to a Gaussian.

for $A_I = 4$ and $A_F = 0$. This highlights the special character of this class of initial states and will be analyzed more quantitatively in the following sections.

A remark is in order on the scaling of the plots shown in Fig. 3 with increasing system size. For the canonical ensemble, it is known that the width of $\rho(E)$, relative to the full width of the spectrum, vanishes in the thermodynamic limit. The question is then what happens for the diagonal ensemble. On general grounds, for Hamiltonians containing only finite-range terms, it was shown in Ref. [27] (supplementary materials) that the width of $\rho(E)$, relative to the full width of the spectrum, also vanishes in the thermodynamic limit. The scaling of the width of $\rho(E)$ depends in this case on the nature of the quench [27]. In Fig. 4, we show a finite size scaling for $\rho(E)$ in the diagonal (a) and canonical (b) ensembles in the quenches from $A_I = 4$ to $A_F = 0$. These results are consistent with the vanishing of the width of $\rho(E)$, relative to the width of the spectrum, as the system size is increased.

IV. ENTROPIES

In the previous section, we have shown that the energy distribution in quenches whose initial states are the ground state of half-filled systems with a superlattice ($A_I \neq 0$) can be well described by a Gaussian, typical of thermal states, as the value of A_I is increased. However, at least for the finite systems we can solve numerically, we showed that such a Gaussian like energy distribution clearly differs from that of the canonical ensemble. In this section, we use the entropies, including the diagonal entropy S_d [35, 36], as a way to quantify the scaling of the energy distributions in all ensembles as the system size is increased. In Ref. [36], it was already shown that the diagonal entropy in integrable systems increases nearly linearly with system size, demonstrating its additive character.

In Fig. 5, we show the entropy per site for two different quenches in half-filled systems, with increasing system size. For both quenches, one can see that all entropy per site plots tend to saturate to a constant value with increasing L , making evident the additivity of this observable in all ensembles. Another result that is apparent from those plots is that S_d is smaller than all other entropies, and it seems that it will remain that way in the thermodynamic limit, as noted in Ref. [36]. An important difference between the behavior of the entropies for a quench from the superlattice to the homogeneous lattice [Fig. 5(a)] and the quench from the homogeneous lattice to the superlattice [Fig. 5(b)] is that, in the former, the entropy of the GGE and the grand-canonical ensemble are nearly identical and the entropies of the GCE and the canonical ensemble approach each other with increasing system size. In the latter quench, the entropies of the GGE and the grand-canonical ensemble differ from each other and their difference is seen to remain constant as the system size is increased. S_{GCE} and S_{CE} approach each other as the system size increases, but their difference is clearly larger than for the $A_I = 2$ to $A_F = 0$ quench.

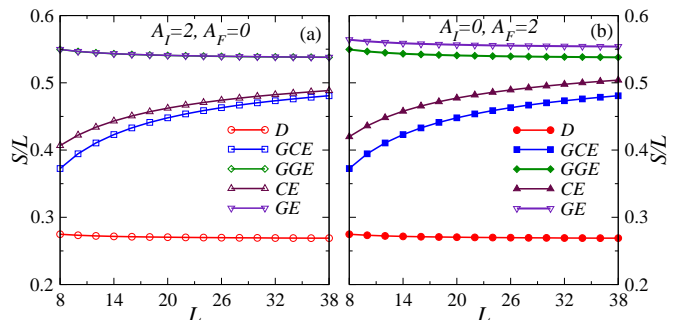


FIG. 5: (Color online) Entropy per site vs. L in quenches from the ground state of a superlattice with $A_I = 2$ to the homogeneous lattice $A_F = 0$ (a) and from the homogeneous lattice $A_I = 0$ to the superlattice with $A_F = 2$ (b). For both quenches, we show results for the diagonal S_d , canonical S_{CE} , grand-canonical S_{GCE} , generalized canonical S_{GCE} , and generalized grand-canonical S_{GGE} entropies. The systems are at half filling $N = L/2$.

In order to quantify the observations above for different quenches and fillings, in Fig. 6 we plot the scaling of $(S_{CE} - S_{GCE})/L$ and $(S_{GE} - S_{GGE})/L$ with system size. The left panels [Figs. 6(a) and 6(b)] depict the results at half filling. Figure 6(a) shows that for any given pair $A_I = x \rightarrow A_F = 0$ and $A_I = 0 \rightarrow A_F = x$, where $x = 2, 4, 6, 8$, the difference $(S_{CE} - S_{GCE})/L$ saturates at greater values for the quenches starting from the homogeneous lattice than for those starting from the superlattice (which, for the lattice sizes shown, still keep decreasing as the system size is increased). The difference $(S_{GE} - S_{GGE})/L$, in Fig. 6(b), exhibits and even more remarkable behavior. It does not change with increasing system size, and it can be seen to be orders of magnitude smaller for the quenches starting from the

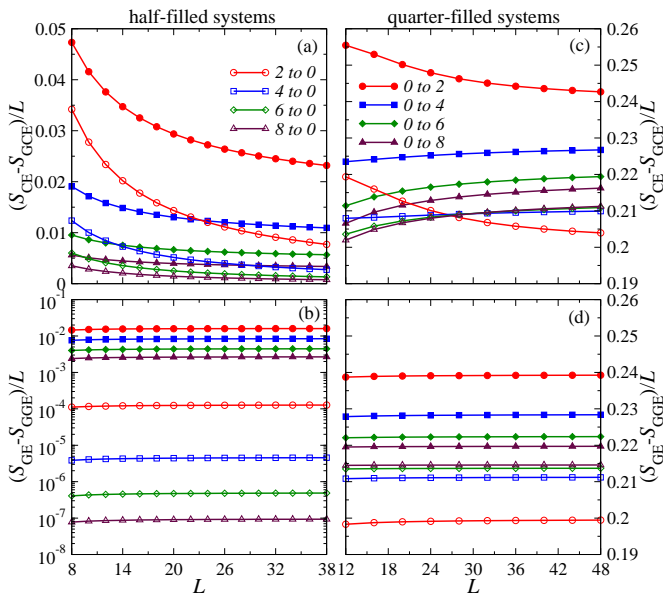


FIG. 6: (Color online) Difference between the entropy of the canonical ensemble and the GCE [(a) and (c)] and between the grand-canonical ensemble and the GGE [(b) and (d)] for quenches at half filling [(a) and (b)] and quarter filling [(c) and (d)]. In all panels, the results for the quenches from the superlattice to the homogeneous lattice are depicted using open symbols, while the ones from the homogeneous lattice to the superlattice are depicted using solid symbols. For the former quenches, results are reported for $A_I = 2$ and $A_F = 0$, $A_I = 4$ and $A_F = 0$, $A_I = 6$ and $A_F = 0$, and $A_I = 8$ and $A_F = 0$, and, for the latter, results are reported for $A_I = 0$ and $A_F = 2$, $A_I = 0$ and $A_F = 4$, $A_I = 0$ and $A_F = 6$, and $A_I = 0$ and $A_F = 8$. In the legend, we use the notation “ A_I to A_F ” to label the plots.

superlattice when compared to those starting from the homogeneous system. The difference $(S_{\text{GE}} - S_{\text{GGE}})/L$ quickly approaches zero as the value A_I in the superlattice is increased. This is exactly the same behavior that was observed in Ref. [8] for the difference between the expectation value of the momentum distribution function (n_k) in the grand-canonical ensemble and that of the time average in the time evolving state. (The latter can be reproduced using the GGE.)

Hence, we can conclude that for the particular class of initial states in Ref. [8], where quenches starting from the ground state of a system with a superlattice lead to expectation values of n_k that approach those in thermal equilibrium as A_I was increased, the sets of states that contribute to the grand-canonical ensemble and the GGE become increasingly similar to each other. Since the GGE describes observables in the integrable system after relaxation [7, 21], thermal ensembles then will also provide a very good estimate for those observables as A_I is increased. From the results in Fig. 6(b), it is important to stress that the entropies in the grand-canonical ensemble and the GGE do not approach each other, for a fixed value of A_I , as the system size is increased.

In Figs. 6(c) and 6(d), we show results for an identical

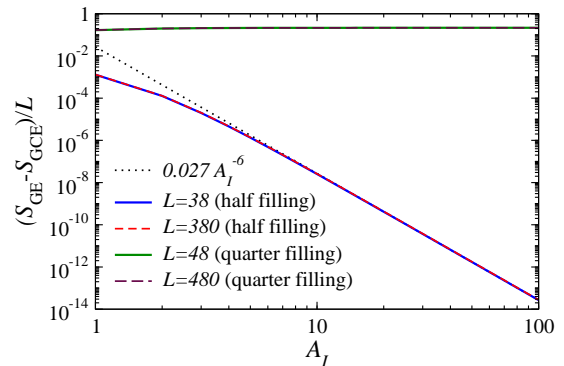


FIG. 7: (Color online) Difference between the entropy of the grand-canonical ensemble and the GGE for quenches at half filling (two lower curves) and quarter filling (two upper curves) vs. A_I . In all cases $A_F = 0$. The dotted line depicts a power-law fit to the large A_I results at half filling. For each quench, results for two different system sizes are presented.

set of quenches as the one in Figs. 6(a) and 6(b) but for systems at quarter filling. For all quenches at quarter filling, one can see that the differences between the entropy in the standard ensembles and in the generalized ones is orders of magnitude larger than for the quenches at half filling. The differences between the two are maximal for the quenches with $A_I \neq 0$. The behavior with changing system size is, however, similar to the one in the systems at half filling. Hence, by comparing all panels in Fig. 6, one can further see that there is something special about the quenches starting from the half-filled superlattice.

As discussed in Refs. [8, 38], the ground state of half-filled systems in a superlattice is insulating and, as the value of A increases, its wavefunction approaches that of a trivial Fock state [a product state of empty (low chemical potential) and occupied (high chemical potential) sites]. In Ref. [8], it was shown that the one-particle correlation length ξ decays as a power law $\xi/a \sim 1/\sqrt{A}/t$ for large values of A/t ($A/t \gtrsim 4$). In Fig. 7, we show how $(S_{\text{GE}} - S_{\text{GGE}})/L$ decreases as A_I increases. Here again, we find a power-law decay for large values of A_I , where $(S_{\text{GE}} - S_{\text{GGE}})/L \sim 1/A_I^6$. This large exponent explains the fast reduction of $(S_{\text{GE}} - S_{\text{GGE}})/L$ seen in Fig. 6 when A_I was increased.

Since for large values of A_I the initial states are nearly uncorrelated states ($\xi \rightarrow 0$), their overlaps with the eigenstates of the final Hamiltonian can be understood to be random and constrained only by energy conservation. This helps in understanding the origin of Gaussian energy distribution observed in the previous section and the closeness of the generalized ensemble entropies to those of the standard ensembles as A_I is increased. In Fig. 6, we also present results for the quenches at quarter filling, where $(S_{\text{GE}} - S_{\text{GGE}})/L$ is seen to saturate to a finite value when A_I is increased. For both fillings, and the system sizes depicted in that figure, finite-size effects can be seen to be negligible.

Confirmation of the conclusions above can be obtained if one realizes that a similar argument applies to the sys-

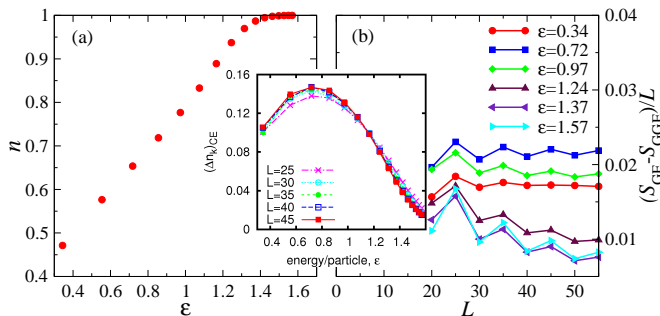


FIG. 8: (Color online) (a) Density in the center of the trap as a function of the excitation energy per particle ϵ , which is changed by increasing V_I in a system with 50 lattice sites and 10 particles. (b) Difference between the entropy of the grand-canonical ensemble and the GGE vs. L for systems with different excitation energy per particle. (Inset): Integrated relative difference between n_k in the diagonal and canonical ensembles (see text) vs. the excitation energy per particle. Results are presented for different system sizes, $L = 25, 30, \dots, 45$ [21].

tems discussed in Ref. [21]. There, the initial state was selected to be the ground state of a trapped system, where [Eq. (1)]

$$V_j^{\text{ext}} = V(j - L/2)^2$$

is a harmonic trapping potential and the evolution was followed after the trap potential V was turned off, *i.e.*, $V_I \neq 0$ and $V_F = 0$. For a fixed number of particles, as V_I increases, a Mott insulator (Fock state for hard-core bosons) with density $n = 1$ forms in the center of the trap. When initial states containing such Mott insulating domains were used for the time evolution, the difference between the momentum distribution function in the diagonal ensemble and standard ensembles of statistical mechanics was seen to decrease [21].

In the inset in Fig. 8, we show the results obtained in Ref. [21] for the integrated difference between the predictions of the diagonal and canonical ensembles for n_k

$$(\Delta n_k)_{\text{CE}} = \frac{\sum_k |\langle \hat{n}_k \rangle_{\text{DE}} - \langle \hat{n}_k \rangle_{\text{CE}}|}{\sum_k \langle \hat{n}_k \rangle_{\text{DE}}},$$

as a function of the excitation energy per particle

$$\epsilon = \frac{E_I - E_G}{N},$$

where E_G is the ground-state energy of the final (homogeneous) Hamiltonian. The excitation energy increases by increasing V_I , while keeping L and N constant [21].

The density in the center of the trap (in the initial state) versus the excitation energy is plotted in Fig. 8(a). There, one can see that $(\Delta n_k)_{\text{CE}}$ (in the inset) is smallest and keeps decreasing when the density in the center of the trap approaches or becomes equal to 1, *i.e.*, when an increasingly large portion of the system comes close or becomes a Fock state.

The scaling of the difference between the entropies in grand-canonical ensemble and the GGE is shown in Fig. 8(b) for different excitation energies. Similarly to the results for the superlattice systems, that difference is seen to be smallest (and decreasing with increasing system size in this case) for the systems whose initial states are closest to Fock states. Hence, once again, a special class of initial states is seen to produce increasingly “thermal-like” observables and generalized ensembles.

V. CONSERVED QUANTITIES

Conserved quantities play a fundamental role in the dynamics and description after relaxation of integrable systems. The latter follows from the evidence that generalized ensembles are able to describe observables after equilibration while standard statistical ensembles are, in general, not [7–14, 16–18, 21–23]. Hence, a distinctive behavior is expected of the distribution of the conserved quantities for those initial states for which observables after relaxation approach thermal values. In this section, we study the behavior of the conserved quantities in those and other cases analyzed in the previous sections.

As explained in Sec. II, the expectation values of the conserved quantities in hard-core boson systems can be straightforwardly computed because they are the occupation of the eigenstates of the noninteracting fermionic Hamiltonian (there are L of those) to which hard-core bosons can be mapped. As such, they can be calculated within the GGE (identical to those of the initial state and the diagonal ensemble by construction) and in the grand-canonical ensemble, for very large lattices. In the grand-canonical ensemble, the occupation of the conserved quantities is dictated by the Fermi distribution

$$\langle \hat{I}_n \rangle_{\text{GE}} = \frac{1}{e^{(\epsilon_n - \mu)/k_B T} + 1}, \quad (20)$$

where ϵ_n are the single-particle eigenenergies.

In Figs. 9(a) and 9(b), we depict the conserved quantities in the GGE (initial state) and the grand-canonical ensemble for quenches at half filling from the ground state in a superlattice to the homogeneous lattice [Fig. 9(a)] and from the ground state of the homogeneous lattice to the superlattice [Figs. 9(b)]. (The conserved quantities are ordered from the highest to the lowest occupied in the initial state.) A clear contrast can be seen between those two panels. In Fig. 9(a) the results for the GGE and grand-canonical ensemble are almost indistinguishable from each other while in Fig. 9(b) they differ from each other markedly. This behavior does not change with increasing system size as, in the same figure, depicted as continuous lines, we also report results for lattices 10 times larger than those used for the calculations depicted as symbols. Qualitatively, these results are similar to those obtained in Ref. [21] for the trapped systems analyzed in the previous section.

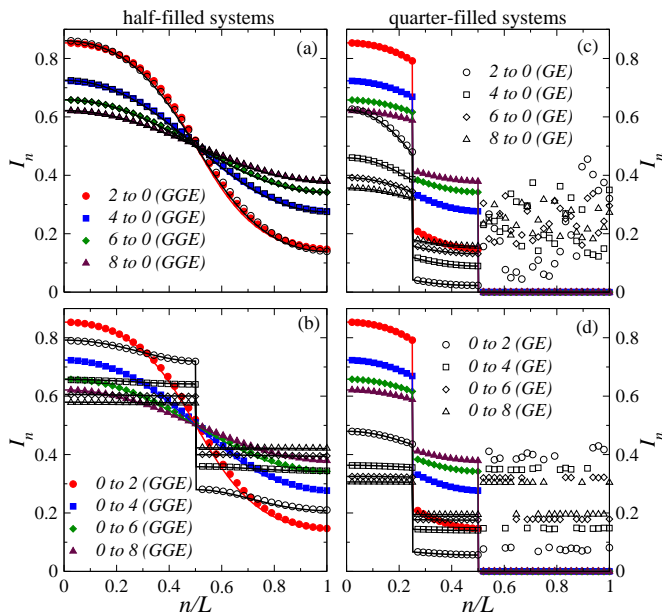


FIG. 9: (Color online) Expectation value of the conserved quantities in quenches from $A_I \neq 0$ to $A_F = 0$ [(a) and (c)] and from $A_I = 0$ to $A_F \neq 0$ [(b) and (d)] for systems at half filling [(a) and (b)] and systems at quarter filling [(c) and (d)]. The conserved quantities are ordered from the highest to the lowest occupied in the initial state. Solid symbols depict the results of the GGE (conserved quantities in the initial state) and open symbols depict the results of the grand-canonical ensemble. The results denoted by symbols (lines) correspond to systems with 38 (380) sites in the half-filled case [(a) and (b)] and with 48 (480) sites in the quarter-filled case [(c) and (d)]. Note that for the smallest system sizes depicted here (the largest analyzed in the previous sections) finite-size effects for the conserved quantities already are negligible. They exhibit an almost perfect overlap with the results in systems 10 times larger. Results are reported for quenches between $A_I = 2$ and $A_F = 0$, $A_I = 4$ and $A_F = 0$, $A_I = 6$ and $A_F = 0$, and $A_I = 8$ and $A_F = 0$ and between $A_I = 0$ and $A_F = 2$, $A_I = 0$ and $A_F = 4$, $A_I = 0$ and $A_F = 6$, and $A_I = 0$ and $A_F = 8$. In the legend, we use the notation “ A_I to A_F ” to label the plots.

Insights into the contrast between the results in Fig. 9(a) and Fig. 9(b) can be gained if one notices that the distribution of conserved quantities for the quenches from and to the superlattice are smooth and identical when A_I in the former is equal to A_F in the latter. This immediately helps one understand why the grand-canonical ensemble prediction of the conserved quantities can match that of the quenches from the superlattice ($A_I \neq 0$) to the homogeneous lattice ($A_F = 0$) but not that of the quenches from the homogeneous lattice ($A_I = 0$) to the superlattice ($A_F \neq 0$). In the former, the final system exhibits no gaps ($A_F = 0$) and the conserved quantities [the Fermi distribution, see Eq. (20)] can be a smooth function of n at finite temperatures, while in the latter the system is gapped ($A_F \neq 0$) and, hence, a discontinuity must occur in the Fermi distribution at the gap position [as seen in Fig. 9(b) for $n/L = 0.5$].

The results reported in Figs. 9(c) and 9(d) for sys-

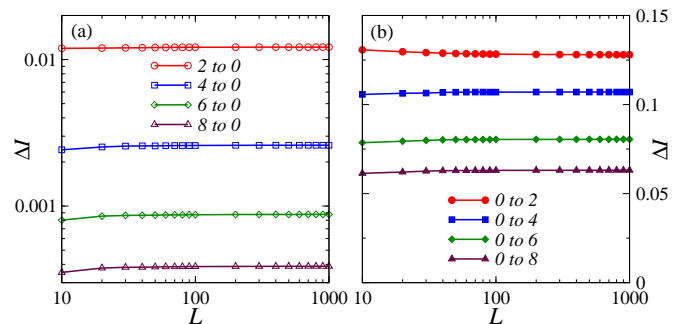


FIG. 10: (Color online) Integrated differences between the conserved quantities in the GGE (initial state) and in the grand-canonical ensemble (see text) vs. L for half-filled systems in quenches from $A_I \neq 0$ to $A_F = 0$ (a) and from $A_I = 0$ to $A_F \neq 0$ (b). Results are reported for quenches between $A_I = 2$ and $A_F = 0$, $A_I = 4$ and $A_F = 0$, $A_I = 6$ and $A_F = 0$, and $A_I = 8$ and $A_F = 0$ in (a); and, between $A_I = 0$ and $A_F = 2$, $A_I = 0$ and $A_F = 4$, $A_I = 0$ and $A_F = 6$, and $A_I = 0$ and $A_F = 8$, in (b). In the legend, we use the notation “ A_I to A_F ” to label the plots.

tems at quarter filling, are qualitatively similar to those in Fig. 9(b). For all quenches, the conserved quantities in the initial state differ substantially from those predicted by the grand-canonical ensemble. The differences can be noted to be particularly large if one realizes that, for many conserved quantities, the initial state has a zero expectation value while the grand-canonical ensemble predicts nonzero, and large, values. This helps in understanding the large differences seen in the previous section between the entropies in the generalized and standard ensembles for the quenches at quarter filling. Once again, the behavior of the conserved quantities in thermal equilibrium is dictated by the Fermi distribution and can be understood given the gapless or gapped nature of the spectrum of the final system.

Figure 10 depicts how the difference between the conserved quantities in the initial state and the grand-canonical ensemble, given by the integrated relative difference

$$\Delta I = \frac{\sum_n |\langle \hat{I}_n \rangle_{\text{GGE}} - \langle \hat{I}_n \rangle_{\text{GE}}|}{\sum_n \langle \hat{I}_n \rangle_{\text{GGE}}},$$

behaves as the system size increases. The results presented, for half-filled systems in quenches from a superlattice potential ($A_I \neq 0$ and $A_F = 0$) in Fig. 10(a) and to a superlattice potential ($A_I = 0$ and $A_F \neq 0$) in Fig. 10(b), show more quantitatively that the results in Fig. 9 do not change with increasing system size.

Figure 10 also makes evident that there is a big quantitative difference between ΔI in the systems whose initial state is the ground state in the superlattice [Fig. 10(a)] and those whose initial state is the ground state of the homogeneous lattice [Fig. 10(b)]. This is better seen in Fig. 11, where ΔI is plotted versus A_I for the former case and versus A_F for the latter. In both cases, we find power-law decays, which are $\sim 1/A_I^3$ when the ini-

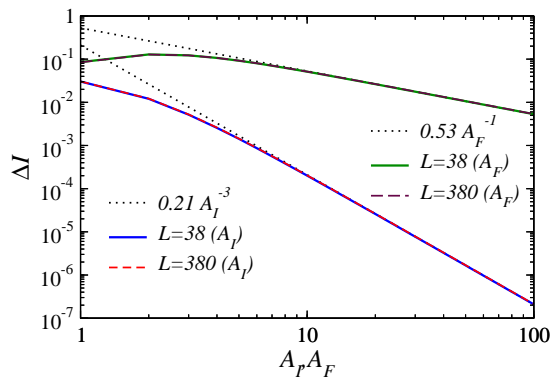


FIG. 11: (Color online) Integrated differences between the conserved quantities in the GGE and in the grand-canonical ensemble. Results are reported for quenches where (i) $A_I \neq 0$ and $A_F = 0$ (two bottom curves) vs. A_I and (ii) $A_I = 0$ and $A_F \neq 0$ (two upper curves) vs. A_F and for two different system sizes. The dotted lines depict a power-law fits to the large A_I , A_F results.

tial state was created for $A_I \neq 0$ and $\sim 1/A_F$ when the final Hamiltonian has $A_F \neq 0$. It is important to stress that while increasing A_I does not qualitatively change the time dynamics of observables of interest, increasing A_F does [8]. In the latter case the damping (relaxation) of the observables is inhibited [8], so the assumption that observables relax to time independent values breaks down.

Finally, from Figs. 10 and 11, we should emphasize once again that, complementary to the behavior seen for $(S_{GGE} - S_{GGE})/L$ in the previous section, the scaling of ΔI versus L is similar for both types of quenches, namely, any finite value of A_I (if $A_F = 0$) or A_F (if $A_I = 0$) leads to a finite ΔI in the thermodynamic limit. The difference between those quenches resides in the actual values of ΔI and their behavior with changing A_I or A_F .

On the basis of those results we can now understand that, for the classes of initial states in Refs. [8, 21] for which observables after relaxation approached thermal values, the control parameter used tuned the distribution of conserved quantities to approach thermal values (resulting in generalized ensembles that, for those states, approach thermal ensembles). This behavior, however, should not be confused with thermalization as understood for nonintegrable systems. For the latter, the difference between observables after relaxation and the predictions of statistical mechanics ensembles is expected to vanish in the thermodynamic limit, while, for the special classes of initial states that we have studied here for integrable systems, such a difference remains finite in the thermodynamic limit for any selected (finite) value of the control parameter.

To conclude, there is an important distinction to be made about the generalized ensembles when compared with standard ensembles of statistical mechanics. In the latter, the conserved quantities (energy, momentum, angular momentum, etc.) are additive and their number is

~ 1 . In the generalized ensembles, the conserved quantities are, strictly speaking, not additive and their number, in the integrable systems considered here, is $\sim L$. The fact that they are not additive can be immediately seen in Fig. 9, where, after making the system size 10 times larger, the value of the conserved quantities does not change. Instead, their number increased by a factor of 10 (that is the reason for plotting the conserved quantities as functions of n/L).

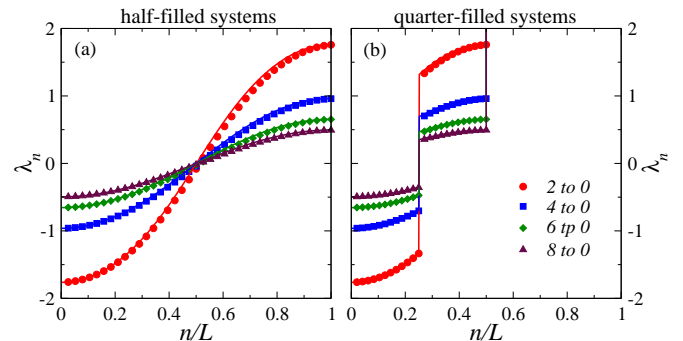


FIG. 12: (Color online) Lagrange multipliers in quenches from $A_I \neq 0$ to $A_F = 0$ for systems at half filling (a) and systems at quarter filling (b). (The results for quenches from $A_I = 0$ to $A_F \neq 0$ are the identical.) Symbols (lines) correspond to systems with 38 (380) sites in the half-filled systems [(a) and (b)] and to systems with 48 (480) sites in the quarter-filled systems. Once again, note that size effects for the Lagrange multipliers are negligible. Results are reported for quenches between $A_I = 2$ and $A_F = 0$, $A_I = 4$ and $A_F = 0$, $A_I = 6$ and $A_F = 0$, and $A_I = 8$ and $A_F = 0$. In the legend, we use the notation “ A_I to A_F ” to label the plots.

In Fig. 12, we show the values of the Lagrange multipliers for the same quenches and system sizes depicted in Fig. 9. As expected from the expression for the Lagrange multipliers [Eq. (12)], they are a smooth function of the values of the conserved quantities (and exhibit negligible finite-size effects in Fig. 12). One can then think of the conserved quantities, considered here to build the generalized ensembles, as additive in a coarse-grained sense. This follows if one realizes that by, increasing the system size, the Lagrange multipliers in a coarse-grained region do not change their values (Fig. 12), but the sum of the expectation values of the conserved quantities in that region (Fig. 9) grows proportionally to the increase of system size. Hence, effectively, the conserved quantities behave as additive. A discussion on the role of additivity of the conserved quantities in generalized ensembles can be found in Ref. [24].

VI. SUMMARY

We have studied the dependence on the initial state of the description of integrable systems after relaxation following a sudden quench. In general, integrable systems are not expected to thermalize. Hence, we have focused on understanding special classes of initial states

that lead to values of observables after relaxation that approach those in thermal equilibrium, when a control parameter is changed. One of our main findings is that, even for such initial states, thermalization does not occur as in nonintegrable systems. In the latter, the difference between the thermal expectation value of an observable and those after relaxation is expected to vanish in the thermodynamic limit. In the integrable systems discussed here, no matter the initial state selected (which is an eigenstate of another integrable system where the control parameter is one of the parameters of the initial Hamiltonian), the distribution of conserved quantities in the thermal ensembles differs from (but can be arbitrarily close to) that of the diagonal ensemble (or the GGE), and the difference does not vanish with increasing system size. Since the values of the conserved quantities constrain the outcome of the relaxation dynamics, the observables after relaxation do not reach thermal values in the thermodynamic limit.

Another of our main findings is that what the control parameter is doing in those special classes of initial states is tuning the distribution of conserved quantities to

approach thermal values. As a result, the initial states exhibit energy densities that are increasingly Gaussian like and entropies of their associated generalized ensembles that approach those of standard ensembles. Similarly to the behavior seen for the conserved quantities, the difference between the entropy per site in the generalized and standard ensembles remains nonzero in the thermodynamic limit. It can, however, be made arbitrarily small by changing the control parameter. Interestingly, for the model considered here, the special initial states were found to be insulating ground states that approach products of single site wavefunctions.

Acknowledgments

This work was supported by the Office of Naval Research and the National Science Foundation under Grant No. DMR-1004268. M.R. thanks A. Polkovnikov and L. F. Santos for useful discussions, and M. Fitzpatrick thanks J. Carrasquilla, E. Malatsetxebarria, and C. Varney for helpful suggestions.

-
- [1] M. Greiner, O. Mandel, T. W. Hänsch, and I. Bloch, *Nature* **419**, 51 (2002).
 - [2] T. Kinoshita, T. Wenger, and D. S. Weiss, *Nature* **440**, 900 (2006).
 - [3] S. Hofferberth, I. Lesanovsky, B. Fischer, T. Schumm, and J. Schmiedmayer, *Nature* **449**, 324 (2007).
 - [4] S. Trotzky, Y.-A. Chen, A. Flesch, I. P. McCulloch, U. Schollwöck, J. Eisert, and I. Bloch, arXiv:1101.2659 (2011).
 - [5] S. R. White and A. E. Feiguin, *Phys. Rev. Lett.* **93**, 076401 (2004).
 - [6] U. Schollwöck, *Rev. Mod. Phys.* **77**, 259 (2005).
 - [7] M. Rigol, V. Dunjko, V. Yurovsky, and M. Olshanii, *Phys. Rev. Lett.* **98**, 050405 (2007).
 - [8] M. Rigol, A. Muramatsu, and M. Olshanii, *Phys. Rev. A* **74**, 053616 (2006).
 - [9] M. A. Cazalilla, *Phys. Rev. Lett.* **97**, 156403 (2006).
 - [10] P. Calabrese and J. Cardy, *J. Stat. Mech.* p. P06008 (2007).
 - [11] M. Cramer, C. M. Dawson, J. Eisert, and T. J. Osborne, *Phys. Rev. Lett.* **100**, 030602 (2008).
 - [12] T. Barthel and U. Schollwöck, *Phys. Rev. Lett.* **100**, 100601 (2008).
 - [13] M. Eckstein and M. Kollar, *Phys. Rev. Lett.* **100**, 120404 (2008).
 - [14] M. Kollar and M. Eckstein, *Phys. Rev. A* **78**, 013626 (2008).
 - [15] D. Rossini, A. Silva, G. Mussardo, and G. E. Santoro, *Phys. Rev. Lett.* **102**, 127204 (2009).
 - [16] A. Iucci and M. A. Cazalilla, *Phys. Rev. A* **80**, 063619 (2009).
 - [17] D. Fioretto and G. Mussardo, *New J. Phys.* **12**, 055015 (2010).
 - [18] A. Iucci and M. A. Cazalilla, *New J. Phys.* **12**, 055019 (2010).
 - [19] J. Mossel and J.-S. Caux, *New J. Phys.* **12**, 055028 (2010).
 - [20] D. Rossini, S. Suzuki, G. Mussardo, G. E. Santoro, and A. Silva, *Phys. Rev. B* **82**, 144302 (2010).
 - [21] A. C. Cassidy, C. W. Clark, and M. Rigol, *Phys. Rev. Lett.* **106**, 140405 (2011).
 - [22] P. Calabrese, F. H. L. Essler, and M. Fagotti, *Phys. Rev. Lett.* **106**, 227203 (2011).
 - [23] M. A. Cazalilla, A. Iucci, and M.-C. Chung, arXiv:1106.5206 (2011).
 - [24] A. Polkovnikov, K. Sengupta, A. Silva, and M. Vengalattore, *Rev. Mod. Phys.* **83**, 863 (2011).
 - [25] J. M. Deutsch, *Phys. Rev. A* **43**, 2046 (1991).
 - [26] M. Srednicki, *Phys. Rev. E* **50**, 888 (1994).
 - [27] M. Rigol, V. Dunjko, and M. Olshanii, *Nature* **452**, 854 (2008).
 - [28] E. Lieb, T. Shultz, and D. Mattis, *Ann. Phys. (NY)* **16**, 406 (1961).
 - [29] T. Holstein and H. Primakoff, *Phys. Rev.* **58**, 1098 (1940).
 - [30] P. Jordan and E. Wigner, *Z. Phys.* **47**, 631 (1928).
 - [31] M. Rigol and A. Muramatsu, *Phys. Rev. A* **72**, 013604 (2005).
 - [32] K. He and M. Rigol, *Phys. Rev. A* **83**, 023611 (2011).
 - [33] M. Rigol, *Phys. Rev. A* **72**, 063607 (2005).
 - [34] M. Rigol and A. Muramatsu, *Mod. Phys. Lett.* **19**, 861 (2005).
 - [35] A. Polkovnikov, *Ann. Phys.* **326**, 486 (2011).
 - [36] L. F. Santos, A. Polkovnikov, and M. Rigol, *Phys. Rev. Lett.* **107**, 040601 (2011).
 - [37] M. Rigol, *Phys. Rev. A* **82**, 037601 (2010).
 - [38] V. G. Rousseau, D. P. Arovas, M. Rigol, F. Hébert, G. G. Batrouni, and R. T. Scalettar, *Phys. Rev. B* **73**, 174516 (2006).